Kinetics of Calcium Carbonate ($CaCO_3$) Precipitation from a Icel-Yavca Dolomite Leach Solution by a Gas (Carbon Dioxide)/Liquid Reaction

by **Mehmet Yildirim***[a]) and **Huseyin Akarsu**[b])

[a]) Department of Mining Engineering, Faculty of Engineering & Architecture, Cukurova University, TR-01330, Balcali, Adana
(phone: +90 322 3387007; fax: +90 322 3386126; e-mail: mehyil@cukurova.edu.tr)
[b]) *Camis Mining Co.*, Is Kuleleri, Kule 3, TR-34300, 4. Levent, Istanbul

The effects of time, CO_2-gas-injection pressure, and bulk temperature on the precipitation of Ca^{2+} ions as a precipitated calcium carbonate (PCC) from a dolomite leach solution were investigated. Precipitation periods from 1 to 7 min were examined, and experiments were run at CO_2-injection pressures of 200–800 kPa. Effects of bulk temperature were studied in the range from 40 to 70°, and precipitation rates of PCC were determined by measuring the Ca^{2+} concentrations in the initial and effluent solutions. Influences of these parameters on the subsequent incorporation of Mg^{2+} ions with the precipitate are discussed in detail. Kinetic analysis of the precipitation was performed by considering the rates as a function of CO_3^{2-}-ion concentrations. Results obtained by this process clearly show that Ca^{2+} ions in the solution can successfully be precipitated as a calcium carbonate product containing 54.70% of CaO and 0.77% MgO, at the rate of 2.01 mM h^{-1}.

1. Introduction. – Precipitated calcium carbonate (PCC) with given characteristics of morphology and particle-size distribution is widely used as filler or pigment for rubber, plastics, paper, prints, *etc*. Currently, PCC is produced by three different processes: a lime soda process, a calcium chloride process, and a carbonation process. In both the lime soda and calcium chloride processes, sodium carbonate is used as the carbonate ion source for the formation of $CaCO_3$ particles.

The carbonation process based on a gas/liquid reaction is most widely used, because it involves cheap raw materials. In this process, crushed limestone is burned in a lime kiln to decompose into calcium oxide and carbon dioxide (*Eqn. 1*). CaO is then hydrated with water to produce a $Ca(OH)_2$ slurry (*Eqn. 2*). The slurry contains undissolved calcium hydroxide, calcium ions, and hydroxide ions. The solubility of $Ca(OH)_2$ decreases as temperature increases. After removing the undissolved impurities, the slurry is fed to a stirring tank at a certain pressure, where it reacts with CO_2 gas and forms calcium carbonate (*Eqn. 3*). This is an energy-intensive process [1].

$$CaCO_3 \rightarrow CaO + CO_2 \; \Delta H\,(1000^\circ) = +165.54 \text{ kJ mol}^{-1} \quad (1)$$

$$CaO + H_2O \rightarrow Ca(OH)_2 \; \Delta H\,(35^\circ) = -65.47 \text{ kJ mol}^{-1} \quad (2)$$

$$Ca(OH)_2 + CO_2 \rightarrow CaCO_{3\downarrow} + H_2O \; \Delta H\,(45^\circ) = -112 \text{ kJ mol}^{-1} \quad (3)$$

Numerous studies have determined the experimental rates of calcium carbonate precipitation [2–6]. The mechanisms of calcite (= polymorph of $CaCO_3$) precipitation

have also been investigated [7][8]. Literature on the precipitation kinetics of calcium carbonate is extensive [2][5][7][9]. Many studies on calcite precipitation and calcite morphology have shown that the presence of Mg^{2+} ions inhibits the rate of calcite precipitation [3][10–12]. Recently, nonequilibrium conditions of Mg^{2+} in foreign-ion incorporation during precipitation have been considered as important factors [11].

This contribution deals with the influence of certain experimental conditions on calcium carbonate precipitation for the removal of Ca^{2+} from a dolomite leach solution, which mainly consists of Ca^{2+}, Mg^{2+}, Cl^-, and H_2O. The removal of Ca^{2+} ions by carbonate precipitation has become a necessity in the preparation of as-clean-as-possible $MgCl_2$ solution to produce high-grade magnesia (MgO). The chemical purity and physical form of MgO should ensure its suitability for high-value metallurgical and chemical applications, and the co-synthesized PCC has both chemical and physical properties which make it acceptable as high-grade carbonate filler in applications such as paper, paints, and plastics.

2. System Description. – Precipitation of $CaCO_3$ by CO_2 absorption is of extensive interest to industrial and geochemical applications. The steps in the absorption reaction mechanism are given by *Eqns. 4–7*. The conversion of CO_2 (g) into CO_2 (aq) or carbonic acid is fast even though not instantaneous (*Eqn. 4*), but the ionic reaction between CO_2 (aq) and OH^- is instantaneous (*Eqn. 5*). HCO_3^- subsequently reacts with OH^- and yields carbonate ion (CO_3^{2-}) and water (*Eqn. 6*). Then, the calcium ions already present in the solution react with CO_3^{2-} ions and precipitate as $CaCO_3$ particles (*Eqn. 7*). Chemical equilibrium favors the presence of CO_3^{2-} above pH 11; both CO_3^{2-} and HCO_3^- form at pH 8–11, whereas below pH 8, only dissolved CO_2 is present. The amount of CO_2, and hence of CO_3^{2-} available for the precipitation reaction, is restricted by the low solubility of CO_2 in water. The used CO_2 flux is substantial so as to provide the gas/liquid reaction. However, after a certain limit, increasing the CO_2 pressure does not have any effect as derived in a previous study [13]. Calcium carbonate precipitation occurs above pH 7.51, whereas the reaction of *Eqn. 8* only occurs above pH 8.70 [14–16]. The precipitation pH can be adjusted with magnesium hydroxide [$Mg(OH)_2$], where the Mg^{2+} ions added are not detrimental to the precipitation and are recovered as $MgCl_2$ in the solution when the precipitation of $CaCO_3$ is completed. Therefore, the overall reaction precipitation is estimated as given in *Eqn. 9*.

$$CO_2\ (g) \rightleftharpoons CO_2\ (aq)\ (\text{or } H_2CO_3) \tag{4}$$

$$CO_2\ (aq) + (OH^-)\ (aq) \rightleftharpoons HCO_3^-\ (aq) \tag{5}$$

$$HCO_3^-\ (aq) + (OH^+)\ (aq) \rightleftharpoons CO_3^{2-}\ (aq) + H_2O \tag{6}$$

$$CO_3^{2-}\ (aq) + Ca^{2+}\ (aq) \rightleftharpoons CaCO_3\ (s) \tag{7}$$

$$Mg^{2+} + CO_3^{2-} \rightarrow MgCO_3 \tag{8}$$

$$CaCl_2 + MgCl_2 + H_2O + Mg(OH)_2 + CO_2 \rightarrow CaCO_3 + 2\ MgCl_2 + 2\ H_2O \tag{9}$$

3. Experimental. – 3.1. *Material and Apparatus.* One reactant used in our experimental works was obtained by HCl leaching of the dolomite sample taken from a deposit in the Yavca area of Icel Province, Turkey. The chloride-leach soln. was 1.73M in Ca^{2+} and 1.58M in Mg^{2+}. Iron and other ionic species were present in trace amounts, and the leach soln. was free from undissolved siliceous particles.

The second reactant, CO_2 gas, was continuously blown into the slurry placed in a stainless-steel vessel (370 ml). Only at the final stage of the reaction, a small flux of CO_2 exited the reactor, which was, however, considerably less than 10% of the provided CO_2. A 35 kg CO_2 tank containing the gas at 50 bar pressure was used as the CO_2 source. The investigation of the formation of precipitated calcium carbonate (PCC) was performed in a three-phase vessel mounted on a scientific-type magnetic stirrer following the overall reaction (*Eqn. 9*). The schematics of the setup are shown in *Fig. 1*. A 370 ml batch reactor was used and equipped with a magnetically-driven impeller allowing the input of high-shear stress into the slurry. The CO_2 pressure applied was controlled by a pressure-measuring device (*Fig. 1*), and the temp. of the precipitation in the reactor was provided by an automatically controlled heater underneath the stainless-steel vessel, which allowed the slurry to be taken out of the device for separation by filtration of the solid $CaCO_3$ particles formed.

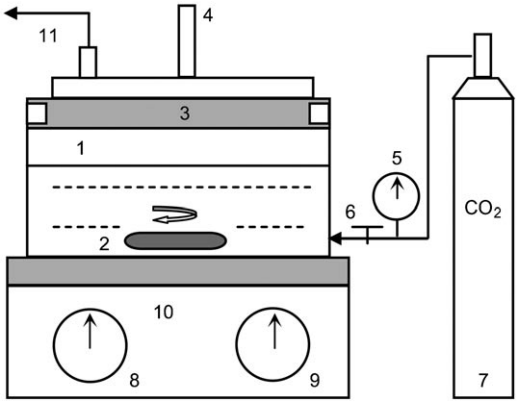

Fig. 1. *Schematic view of the experimental setup.* 1) Stainless-steel vessel containing the leach solution. 2) Magnetically driven stirrer. 3) Lid. 4) Support. 5) CO_2-Pressure controller. 6) CO_2-Inlet controller. 7) CO_2 Tank. 8) Stirring-rate controller. 9) Temperature-controlling unit. 10) Automatically controlled heater. 11) Temperature and pH measurements.

3.2. *Procedure.* A predetermined amount of the leach soln. (60 ml) was placed into the vessel, and the heating temp. was adjusted as required (°C). Then, the pH of the soln. was adjusted to 10 with $Mg(OH)_2$. After allowing CO_2 injection at a certain pressure, the stirrer was started. The stirring rate was kept constant at 1000 rpm for all the runs. At the beginning and the end of each experiment, an aliquot of the leach soln. was sampled with a plastic syringe, and the particles formed were filtered through a *Millipore-R* 0.45 μm filter and stored, after drying and weighing, in a plastic tube for later analysis. The chemical composition of the PCC was determined by means of the *RIX-3000-Rigaku* X-ray and *SRS-3000-Siemens* X-ray fluorescence spectrometers. Calcium and magnesium concentrations of the solns. were determined by a *Perkin-Emler-2380* atomic-absorbtion spectrometer. The specific surface area and particle size for the PCC sample obtained under optimum conditions were determined with the *Sympatec-Helos(H0901)-Rodos* size-analysis device, which is based on the gas-permeability laser-diffraction method. Color analysis was conducted with the *Lange-Micro-Color* device [16].

The precipitation of $CaCO_3$ (PCC) from this leach soln. was assumed to be as presented by *Eqn. 7*. When $CaCO_3$ precipitation occurs, the experimental precipitation rate R can be determined from the

calcium-ion-concentration change as a function of time according to *Eqn. 10*, where t represents the precipitation time.

$$R = d[Ca^{2+}]/dt \text{ [mM h}^{-1}\text{]} \quad (10)$$

4. Results and Discussion. – 4.1. *Effect of Time.* The experimental data plotted in *Fig. 2* show that an increase in the precipitation period caused a decrease in the precipitation rate R and an increase in precipitation recovery. The recovery reached 96.53% after 5 min when $\log R$ was 4.30 [mM h^{-1}]. As time increased also the concentration of Ca^{2+} ions in the solution decreased (*Fig. 3*). Three different time intervals can be identified in the curve corresponding to the Ca^{2+}-ion concentrations. The first interval, up to 1 min, possibly represents a rapid increase in nucleation at initial Ca^{2+} concentration. In this interval, the formation of PCC was fast. The second

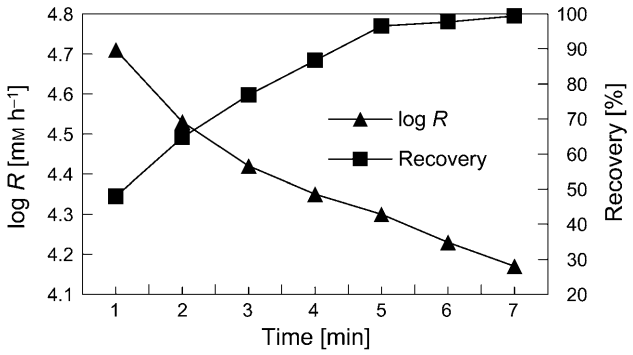

Fig. 2. *Log* R (R = precipitation rate) *and recovery of* Ca^{2+} *ions under equilibrium conditions in the solution as a function of time* (70°, CO_2 pressure 200 kPa)

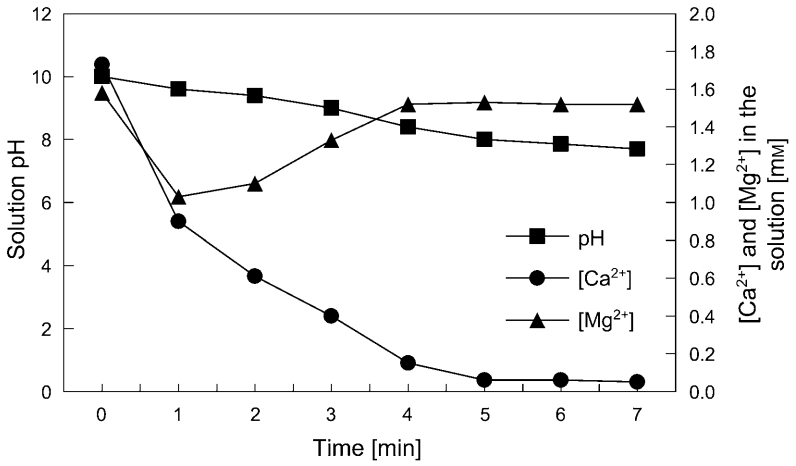

Fig. 3. *Changes in pH,* $[Ca^{2+}]$*, and* $[Mg^{2+}]$ *in the effluent solution as a function of time* (70°, CO_2 pressure 200 kPa)

interval may be considered as a linear growth period during which CO_3^{2-} consumption was constant as its rate of production from CO_2 injection was balanced by its conversion to PCC. Previous researchers have obtained similar results [17]. In the third interval, corresponding to the period between 5 and 7 min, precipitation recovery reached 97.10%. On the other hand, the $[Mg^{2+}]/[Ca^{2+}]$ ratio in the solution continuously increased and reached 30.40 after 7 min (*Table 1*).

Table 1. *Changes of pH, $[Ca^{2+}]$, and $[Mg^{2+}]$ in the Solution, Precipitation Recoveries of Ca^{2+} Ions, and CaO and MgO Contents of the PCC Obtained as a Function of Time at 70° and 200 kPa CO_2 Pressure*

Time [min]	Solution pH	$[Ca^{2+}]$ [M]	CaO [%]	$[Mg^{2+}]$ [M]	MgO [%]	$[Mg^{2+}]/[Ca^{2+}]$	Recovery [%]
0	10.00	1.73		1.58		0.91	
1	9.60	0.90	37.60	1.03	17.71	1.14	47.90
2	9.40	0.61	42.80	1.10	13.38	1.80	62.50
3	9.00	0.40	49.80	1.33	6.70	3.33	74.40
4	8.40	0.15	53.40	1.52	1.40	10.13	81.60
5	8.00	0.06	54.70	1.53	0.77	25.50	94.80
6	7.86	0.06	54.70	1.52	1.59	25.33	94.80
7	7.70	0.05	55.03	1.52	1.58	30.40	97.10

It is shown in *Fig. 3*, that the Mg^{2+} concentration in the solution decreased to 1.03M within 1 min, and then increased again. In other words, the highest amount of Mg^{2+}-ion incorporation took place in this period (*Table 1*). The lowest Ca^{2+} concentration and highest Mg^{2+} concentration in the solution were observed after 5 min. This points out that Mg^{2+} ions associated with $CaCO_3$ precipitated first, then as time proceeded, they slowly detached again into the solution. From *Table 1*, the MgO content of the precipitate decreased from 17.71 to 0.77% after 1 and 5 min, respectively. The subject is entirely related to the crystal growth of calcite in the presence of Mg^{2+} ions, which decreases the rate of calcite growth in steps through an incorporation-induced increase in solubility rather than by physically blocking their migration [11].

Hydration enthalpies of Ca^{2+} and Mg^{2+} ions are different, and a hydrated Mg^{2+} ion absorbed on a calcite surface site will remain for a relatively long period without dehydration and incorporation into the structure in comparison with a Ca^{2+} ion. The bond between H_2O and free Mg^{2+} ions is stronger than that between Mg^{2+} and the calcite surface. The initial addition of a first layer of Mg^{2+} is an exothermic process, but the addition of a second layer is markedly less exothermic, which suggests that the proceeding of Mg^{2+} accumulation in steps will become an endothermic process after a few layers of Mg^{2+} have formed and are inhibited. The differences in the dehydration properties of Ca^{2+} and Mg^{2+} support a reaction in which Mg^{2+} consumes carbonate O-atoms exposed at the calcite surface to complete its hydration shell, and its surface detachment destabilizes the surface hydration layer and provides a mechanistic opportunity for a subsequent detachment of lattice ions at defect sites. The results are in agreement with those obtained by other researchers [3][10]. *Eqn. 11* shows that hydrogencarbonate ions (HCO_3^-) act as an additional reservoir for H^+ ions, but no change in the overall pH occurs unless the carbonate ions are precipitated as calcium carbonate. *Eqn. 11* shifts to the right as the pH of the solution increases. It was observed

that as precipitation of the carbonate ions proceeded, lower pH measurements were recorded, because of the increase in H^+ concentration in the solution. This is consistent with the results obtained (*Fig. 3*).

$$HCO_3^- \rightleftharpoons CO_3^{2-} + H^+ \tag{11}$$

4.2. *Effect of CO_2-Gas Pressure. Fig. 4* shows the influence of CO_2-injection pressure on the precipitation rate *R* at constant temperature and time. As the injection pressure increased, the precipitation rate decreased. The highest and lowest rates were observed at the pressures of 200 and 800 kPa, respectively. *Eqns. 4–7* indicate that the CO_3^{2-} concentration increases with an increase of the gas-injection pressure. Hence, the $[CO_3^{2-}]/[Ca^{2+}]$ ratio increases in the solution. However, the precipitation of calcite is closely related to the super saturation Ω for the CO_3^{2-}- and Ca^{2+} ions given by *Eqn. 12*, where K_{sp} is the solubility product constant for $CaCO_3$, and the higher the $'\Omega$, the more likely the precipitation is to take place. Low precipitation rates were obtained at high $[CO_3^{2-}]/[Ca^{2+}]$ ratios by earlier researchers [18]. It was determined that as the injection pressure increased, the negative-charge density on the crystal increased, which created more reactive sites for crystal growth. Also, an increase in injection pressure was associated with a decrease in pH and an increase in ionic strength at a constant degree of thermodynamic super saturation with respect to the calcite [19]. An increase in the negative charge of $CaCO_3$ crystals and a decrease in the associating capacity of dissolved inorganic carbon (DIC) due to a decrease in solution pH may be on account of the lower inhibitory effect of DIC at higher injection pressures. However, in the surface speciation model, an increase in injection pressure possibly caused an increase in carbonate-bearing species on the mineral surfaces, which was effective on crystal growth and dissolution [18]. Therefore, both $CaCO_3$-crystal growth and dissolution from the surfaces increase with injection pressure. An imperative consequence of increasing the amount of CO_2 absorbed in the solution is the enlargement of the amount of tiny particles of amorphous calcium carbonate. It has higher solubility than that of crystalline calcium carbonate [13].

$$'\Omega = [CO_3^{2-}][Ca^{2+}]/K_{sp} \tag{12}$$

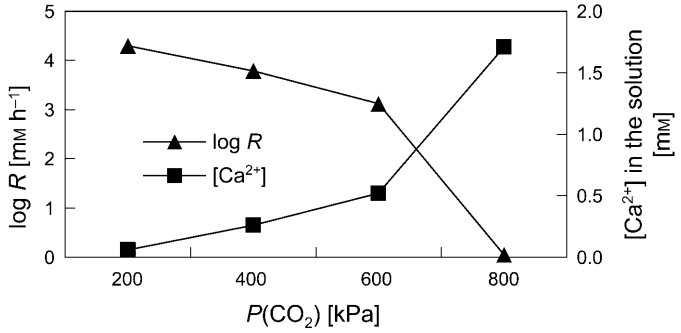

Fig. 4. *Log* R (*R* = precipitation rate) *and Ca^{2+} concentration as a function of the experimentally applied CO_2 pressure* (70°, *t* 5 min)

Fig. 5 shows changes in the CaO and MgO content of the precipitates as a function of the applied CO_2 pressure. The CaO content of the precipitate decreased as pressure increased, but the decrease was not significant up to a gas pressure of 600 kPa. However, the situation was *vice versa* for the MgO content. When the pressure was 200 kPa, the highest CaO content (54.70%) and the lowest MgO content (0.77%) could be obtained. Hence, the need to increase pressure beyond 200 kPa never arises. From the curve representing the MgO content, the highest magnesium incorporation (51.25%) was observed at a pressure of 800 kPa. As observed from thermodynamic calculations, $MgCO_3$ precipitation begins above pH 10.45, whereas it is pH 7.51 for $CaCO_3$ precipitation. Therefore, the incorporation of Mg^{2+} ions with the precipitate enhanced with an increase in CO_2-injection pressure. Probably a higher density of $MgCO_3$ than that of $CaCO_3$ was effective in the co-precipitation of Mg^{2+} ions during the crystal-growth period at a pressure of 800 kPa [10][11].

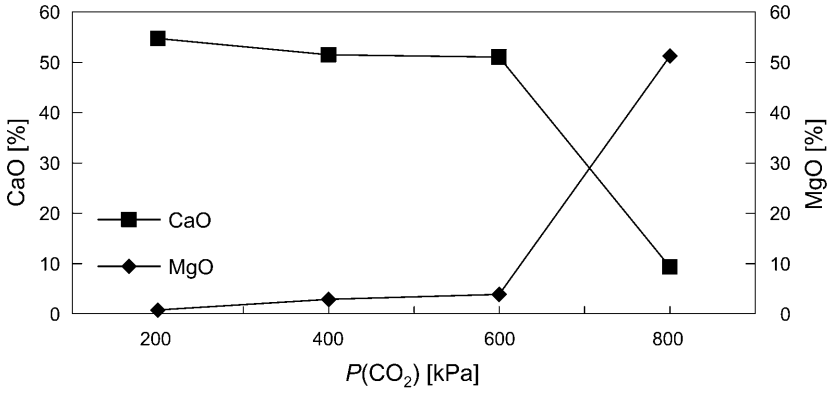

Fig. 5. *CaO and MgO Contents of the precipitates* vs. *the experimentally applied CO_2 pressure* (70°, *t* 5 min)

4.3. *Effects of Temperature.* When heating the solution, the equilibrium between hydrogencarbonate and carbonate shifts toward the carbonate ion (*Eqn. 11*). However, the increasing temperature negatively affects the CO_2 solubility in H_2O, *i.e.*, *Eqn. 4* shifts to the left, but positively affects the formation of amorphous $CaCO_3$ as its solubility is inversely related to temperature. *Fig. 6* shows that the precipitation rate *R* increased and the Ca^{2+} concentration decreased in the solution as a function of increasing temperature. The log *R* achieved was 4.30, and the Ca^{2+} concentration was only 0.06M when the temperature was 70°.

The temperature was also significant for the curves representing the CaO and MgO contents of the precipitates (*Fig. 7*). At lower temperatures, it is possible that Ca^{2+} ions hydrate more strongly, the behavior akin to Mg^{2+} ions, thereby increasing the energy necessary to form anhydrous $CaCO_3$ phases. However, at higher temperatures (in this case 70°), the solubility of $CaCO_3$ is greater than that of the underlying low-magnesium-bearing calcite substrate; as a result, a low precipitation rate was observed [11][16]. At 70°, the highest precipitation rate and the lowest MgO percentage were

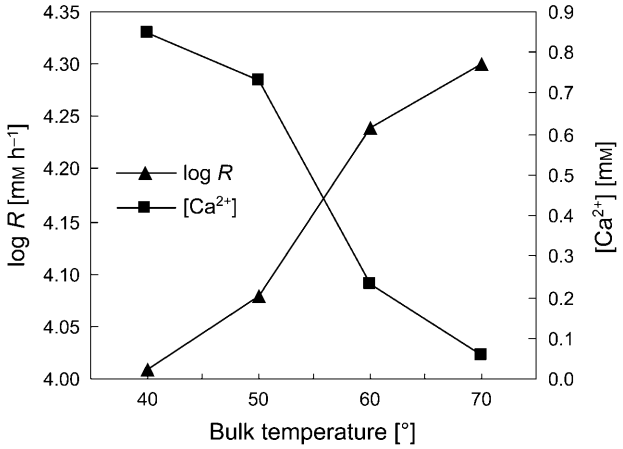

Fig. 6. *Log* R (*R* = precipitation rate) *and* Ca^{2+} *concentration under equilibrium conditions in the solution as a function of bulk temperature* (CO_2 pressure 200 kPa, *t* 5 min)

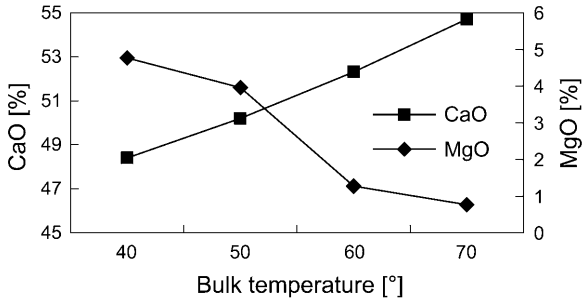

Fig. 7. *CaO and MgO Contents of the precipitate as a function of bulk temperature* (CO_2 pressure 200 kPa, *t* 5 min)

observed. In other words, at this operating temperature, the highest amount of Ca^{2+} ions was precipitated as the $CaCO_3$ particles contained only 0.77% MgO, while leaving behind the $MgCl_2$ solution purified from Ca^{2+} ions.

4.4. *Kinetic Analysis of the Precipitation.* In this study, the initial calcium concentration was kept constant for each run, and the net experimental rate *R* was described only with respect to carbonate ion (*Eqn. 13*; *cf. Eqn. 10* and *14*). Taking the logarithmic form of *Eqn. 13* yields *Eqn. 15*, where *k* is the precipitation-rate constant and *n* is an apparent reaction order. The logarithms of the experimental rates, $\log(d[Ca^{2+}]/dt)$, were plotted against the $\log[CO_3^{2-}]$ values obtained by calculations from the precipitation equilibrium conditions for different times (1–7 min) and temperatures (40, 50, 60, and 70°). According to a second-order reaction (*Eqn. 14*) between Ca^{2+} and CO_3^{2-}, the plot of $-\log(d[Ca^{2+}]/dt)$ *vs.* $\log[CO_3^{2-}]$ should yield a straight line with slope *n* and intercept $-\log k$ (*Fig. 8*).

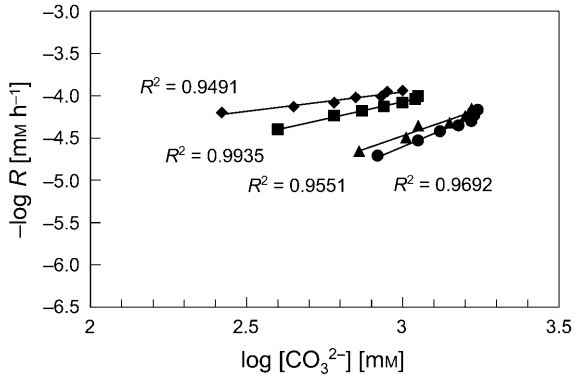

Fig. 8. *– Log* R (*R* = precipitation rate) *as a function of log[CO_3^{2-}] under equilibrium conditions for different times* (1–7 min) *and temperatures* (◆, 40°; ■, 50°; ▲, 60°, ●, 70°) (CO_2 pressure 200 kPa; R^2 = correlation coefficient)

$$R = k\,[CO_3^{2-}]^n \quad [\text{mM h}^{-1}] \tag{13}$$

$$d[Ca^{2+}]/dt = k\,[CO_3^{2-}]^n \tag{14}$$

$$\log R = \log k + n \log[CO_3^{2-}] \tag{15}$$

Fig. 9 shows an *Arrhenius*-type, semi-logarithmic plot of the slopes of the linear regression lines in *Fig. 8 vs.* reciprocal temperature. In this figure, the slope of the curve is equal to $-E_a/2303R$, and its intercept is $\ln A$ (R = gas constant). The slope of the linear curve depicted in *Fig. 9* is consistent with an apparent activation energy, *i.e.*, E_a = 136.5 kJ mol^{-1}; this value is relatively high and points to a surface-controlled mechanism for the precipitation of $CaCO_3$. These experiments confirm a strong temperature dependence of the precipitation reactions in this process. The activation energy obtained from precipitation experiments carried out at 25, 35, and 45° in the aqueous solution was 155 kJ mol^{-1} [19]. In another research, it was found to be 55 kJ mol^{-1}, and according to literature, the E_a value is usually between 39 and 155 kJ mol^{-1} [20].

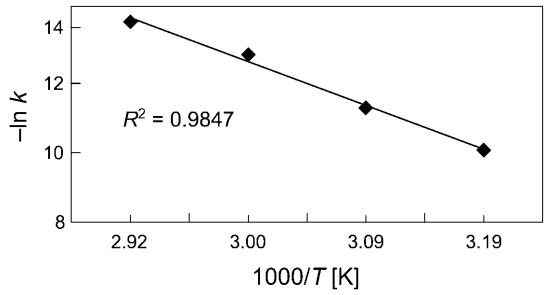

Fig. 9. Arrhenius *plot for the precipitation of calcium carbonate particles*

The results obtained in this study show that the reaction order n increases and the rate constant k decreases as a function of temperature at constant time and CO_2 pressure (*Table 2*). The increase in reaction order with respect to carbonate concentration proposes a change in the mechanism of calcium carbonate precipitation. However, a decrease in the rate constant could be attributed to an increase in the ratio of $[Mg^{2+}]/[Ca^{2+}]$ in the solution during precipitation as time proceeds.

Table 2. *Precipitation Rates and Reaction Orders* n *for Various Temperatures* (40, 50, 60, and 70°) *at 200 kPa CO_2 Pressure* (*Fig. 8*)

Temperature [°]	$-\log k$ [mM h^{-1}]	n
40	4.40	0.57
50	4.98	0.90
60	5.80	1.25
70	6.20	1.42

4.5. *Analysis of the PCC and Leach Solution* ($MgCl_2$). The $d_{0.50}$ and $d_{0.90}$ of the PCC detected were 3.54 and 7.20 μm, respectively. However, natural ground calcium carbonate (GCC) had a wider particle-size distribution. Its $d_{0.50}$ and $d_{0.90}$ were 7.62 and 23.48 μm. The color property was determined with the following color grades: whiteness 99.70; redness: 0.70; yellowness: 2.10.

The particle-size range used in the paint industry is 1 – 40 μm, and the commonly accepted particle size is less than 5 μm. The minimum whiteness for a commercial PCC product used in paints, plastics, and paper industry should be at least 95.00, and the minimum $CaCO_3$ content should be 95 – 98%, and the maximum Fe_2O_3 content 0.20%. The other undesirable oxide in the PCC product is SiO_2, which should not exceed 0.20%. The magnesium ion associated is usually present, and its tolerable content is *ca.* 2.00% [16]. The chemical analysis of our PCC is shown in *Table 3*.

Table 3. *Chemical Analysis of the Optimum Precipitated Calcium Carbonate* (PCC)

Component	CaO	MgO	SiO_2	Fe_2O_3	Al_2O_3	CO_2	SO_4	Sr	Li	B	Ti	Mn
Amount [%]	54.70	0.77	0.04	0.03	0.02	44.37	0.13	0.01	< 0.002	< 0.002	< 0.002	< 0.002

As shown in *Fig. 10*, the particle-size distribution of the PCC sample is narrower than the GCC sample. The SEM (scanning-electron microscope) observations of the obtained precipitate show agglomerates of particles displaying a scalenohedral habit. The purified leach solution ($MgCl_2$) contained 0.06M Ca^{2+} and 3.45M Mg^{2+}.

5. Conclusions. – Precipitation and removal of Ca^{2+} ions from dolomite leach solutions obtained by HCl acid/dolomite leaching can successfully be performed by using the experimental setup and procedure described in this work. As a result, the dolomite leach solution mostly consisting of $MgCl_2$ can be cleaned off the Ca^{2+} ions present. Good results were obtained at 200 kPa CO_2-injection pressure, 70° bulk temperature, and a 5 min precipitation period. Under these conditions, the precipitation rate (for Ca^{2+} ions) reached $2.01 \cdot 10^4$ (mM h^{-1}), and the lowest MgO content incorporated with PCC was 0.77%. The precipitation rate was tightly regulated by the

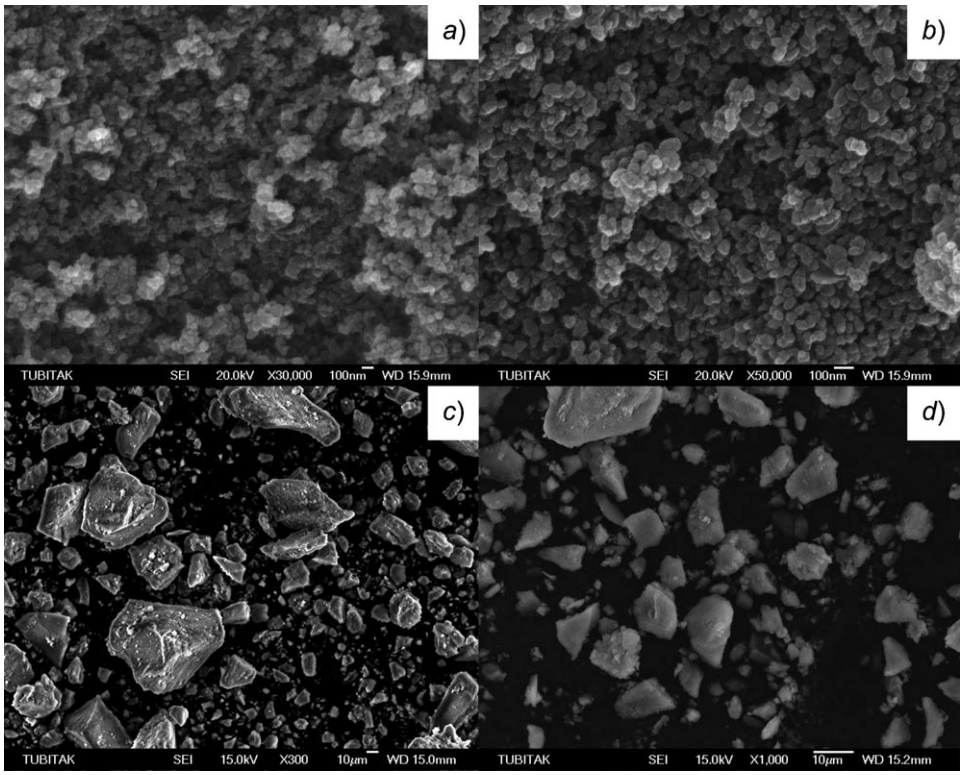

Fig. 10. *SEM Micrographs of $CaCO_3$ particles:* a) *and* b) *Precipitated calcium carbonate* (PCC) *samples obtained at 70°* (pH 8.40; *t* 5 min; CO_2 pressure 200 kPa), *and* c) *and* d) *natural ground calcium carbonate* (GCC) *samples*

$CaCO_3$ saturation state and pH of the solution; it decreased with an increase in CO_2-injection pressure.

The apparent activation energy of the formation of PCC from the dolomite leach solution was determined to be 136.5 kJ mol^{-1}. The utilization of CO_2 gas in this process will cause a reduction of CO_2 emissions into the atmosphere. If CO_2 gas is captured under economic conditions from a suitable source, the precipitation of Ca^{2+} ions as PCC, which is a commercial grade obtained from dolomite leach solutions free from detrimental ionic species, will be feasible. An upgraded solution containing 0.06M Ca^{2+} and 3.45M Mg^{2+} was obtained from the leach solution by the carbonation process based on the described gas (CO_2)/liquid (leach solution) reaction.

The authors thank the referee for thoroughly reviewing this article and giving valuable suggestions.

REFERENCES

[1] S. Teir, S. Eloneva, R. Zevenhoven, *Energy Convers. Manage.* **2005**, *46*, 2954.
[2] W. Dreybrodt, L. Eisenlohr, B. Madry, S. Ringer, *Geochim. Cosmochim. Acta* **1997**, *61*, 3897.
[3] M. Deleuze, S. L. Brantley, *Geochim. Cosmochim. Acta* **1997**, *61*, 1475.

[4] R. Shiraki, S. L. Brantley, *Geochim. Cosmochim. Acta* **1995**, *59*, 1457.
[5] P. Zuddas, A. Mucci, *Geochim. Cosmochim. Acta* **1994**, *58*, 4353.
[6] S. Zhong, A. Mucci, *Geochim. Cosmochim. Acta* **1993**, *57*, 1409.
[7] I. Lebron, D. L. Suarez, *Geochim. Cosmochim. Acta* **1997**, *62*, 405.
[8] P. M. Dove, M. F. Hochella, *Geochim. Cosmochim. Acta* **1993**, *57*, 705.
[9] C. A. Brown, R. G. Compton, C. Narramore, *J. Colloid Interface Sci.* **1993**, *160*, 372.
[10] R. S. Arvidson, M. Collier, K. J. Davis, M. D. Vinson, J. E. Amonette, A. Luttge, *Geochim. Cosmochim. Acta* **2006**, *70*, 583.
[11] K. J. Davis, P. M. Dove, L. E. Wasylenki, J. J. De Yoreo, *Am. Mineral.* **2004**, *89*, 714.
[12] Y. Zhang, R. A. Dawe, *Chem. Geol.* **2000**, *163*, 129.
[13] C. Domingo, E. Loste, J. Gomez-Morales, J. Garcia-Carmona, J. Fraile, *J. Supercrit. Fluids* **2006**, *36*, 202.
[14] R. C. Patel, F. Garland, G. Atkinson, *J. Solution Chem.* **1975**, *4*, 161.
[15] G. M. Anderson, D. A. Crerar, 'Thermodynamics in Geochemistry: The Equilibrium Model', Oxford University Press, New York, 1993, p. 146–154.
[16] H. Akarsu, Ph.D. Thesis, Cukurova University at Adana, 2004.
[17] S. Rigopoulos, A. G. Jones, *Chem. Eng. Sci*. **2001**, *56*, 6177.
[18] O. Nilsson, J. Sternbeck, *Geochim. Cosmochim. Acta* **1999**, *63*, 217.
[19] P. G. Koutsoukos, C. G. Kontoyannis, *J. Chem. Soc., Faraday Trans. 1* **1984**, *80*, 1181.
[20] L. Brecevic, D. Kralj, *Croat. Chem. Acta* **2007**, *80*, 467.

Received August 3, 2008